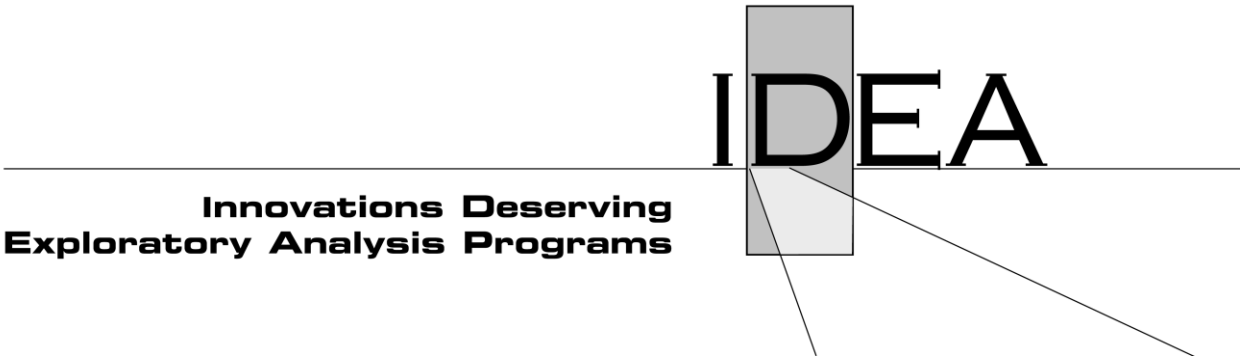

Transit IDEA Program

Advanced Neutral Temperature Estimation using Solitary Waves (ANTEUSW)

Final Report for
Transit IDEA Project 86

Prepared by:
Piervincenzo Rizzo, University of Pittsburgh
Amir Nasrollahi, University of Pittsburgh

January 2019

TRB TRANSPORTATION RESEARCH BOARD
The National Academies of
SCIENCES · ENGINEERING · MEDICINE

Innovations Deserving Exploratory Analysis (IDEA) Programs Managed by the Transportation Research Board

This IDEA project was funded by the Transit IDEA Program.

The TRB currently manages the following three IDEA programs:

- The NCHRP IDEA Program, which focuses on advances in the design, construction, and maintenance of highway systems, is funded by American Association of State Highway and Transportation Officials (AASHTO) as part of the National Cooperative Highway Research Program (NCHRP).
- The Rail Safety IDEA Program currently focuses on innovative approaches for improving railroad safety or performance. The program is currently funded by the Federal Railroad Administration (FRA). The program was previously jointly funded by the Federal Motor Carrier Safety Administration (FMCSA) and the FRA.
- The Transit IDEA Program, which supports development and testing of innovative concepts and methods for advancing transit practice, is funded by the Federal Transit Administration (FTA) as part of the Transit Cooperative Research Program (TCRP).

Management of the three IDEA programs is coordinated to promote the development and testing of innovative concepts, methods, and technologies.

For information on the IDEA programs, check the IDEA website (www.trb.org/idea). For questions, contact the IDEA programs office by telephone at (202) 334-3310.

IDEA Programs
Transportation Research Board
500 Fifth Street, NW
Washington, DC 20001

Advanced Neutral Temperature Estimation using Solitary Waves (ANTEUSW)

IDEA Program Final Report
For the period 05/2017 through 12/2018
Transit IDEA Project 86

Prepared for the Transit IDEA Program
Transportation Research Board
The National Academy of Sciences, Engineering, and Medicine

Piervincenzo Rizzo, Ph.D.
Professor,

Amir Nasrollahi, Ph.D.
Postdoctoral Researcher

Department of Civil and Environmental Engineering
University of Pittsburgh, Pittsburgh, Pennsylvania

January 2019

ACKNOWLEDGEMENTS

The work presented in this report was supported by the U.S. National Academy of Sciences, Engineering, and Medicine through the Transit IDEA program, project T-86. The opinions expressed in this report are solely of its authors and the U.S. National Academy of Sciences and the US Government do not necessarily concur with, endorse, or adopt the findings, conclusions and recommendations either inferred or expressly stated in the report.

The authors acknowledge the help of Mr. Charles Hager, full-time technician in the Department of Civil and Environmental Engineering at the University of Pittsburgh, for his support and guidance in the preparation of the setups and the execution of the experiments. The authors are also grateful to Norfolk-Southern Corporation for the donation of the rails used in the experiments. The guidance of Dr. Velvet Basemera-Fitzpatrick throughout the duration of the project was greatly appreciated.

The TRB Expert Panel consisted of members and associates of the Transportation Research Board (a part of the National Academies of Sciences, Engineering, and Medicine) and members of the Academia. The Expert Panel members - all of which are recognized individuals in the transit industry or in the Academia - have provided valuable feedbacks by reviewing the quarterly reports and by conference calls. Drs. Rizzo and Nasrollahi sincerely acknowledge the Expert Panel members (in alphabetical order):

Dr. Ivan Bartoli, Associate Professor, Drexel University;

Mr. Melvin Clark, LTK Engineering Services;

Mr. Brad Kerchof, Director Research and Tests, Norfolk Southern Corporation;

Mr. Nathan Leventon, American Public Transportation Association;

Dr. David Thurston, Chief Engineer – Train Control, Canadian Pacific Railway;

Dr. Jinkyu "JK" Yang, Associate Professor, University of Washington.

TABLE OF CONTENTS

EXECUTIVE SUMMARY

ENGINEERING NEED. Continuous welded rails (CWRs) are widely used in rail transportation. Typically, they are laid under tension in order to counteract the thermal expansion that occurs in warm days. Ideally the state of stress is such that the rail neutral temperature (RNT), i.e. the temperature at which the net stress in the rail is zero, is comprised between 90°F and 110°F. Over the years, operational conditions and maintenance result in the decrease of the RNT to an unknown value, increasing the risk of buckling, a structural problem that causes several derailments every year.

As the accurate knowledge of the RNT or of the current stress helps rail operators to estimate the temperature at which a rail will likely buckle, there is a need for a reliable nondestructive evaluation (NDE) methods able to estimate the neutral temperature or the longitudinal stress of CWRs anytime and anywhere along the rail network.

PROPOSED SOLUTION. To address this need, a new NDE method able to determine the axial stress and the neutral temperature of CWRs is investigated. The method relies on the propagation of highly nonlinear solitary waves along a device, hereinafter called the *transducer*, placed in a dry point contact with the rail to be inspected. The *transducer* contains a chain of spherical particles at one end of which, a solitary wave is generated. Once the wave reaches the opposite end, which is in contact with the rail, it is reflected back giving rise to one or more pulses. The research hypothesis investigated in this T-86 project is that the axial stress affects the number, amplitude and speed of the reflected pulses. As such, the new NDE method aims at measuring the axial stress in rails using a simple "plug-and-play" device, the *transducer*, within which the solitary waves propagate. The neutral temperature is then estimated using an empirical equation.

PERFORMED RESEARCH. To validate the research hypothesis, a generalized finite element analysis was developed and coupled to a discrete particle model to predict how some characteristics of solitary waves are affected by the stress in the CWRs. A few experiments were also conducted to design a practical and cost-effective *transducer* able to provide repeatable measurements, and to validate the models in a laboratory setting.

FINDINGS. It was found that: (1) the *transducers* necessary to apply the NDE method are easy to assemble, inexpensive, practical and the measurements they provide are repeatable; (2) some wave features such as the amplitude and the time of flight of the reflected waves are monotonically dependent on the rail longitudinal stress, provided that the structural behavior of CWRs is equivalent to a straight beam a few meters long at least; (3) the monotonic relationship between wave features and axial stress can be used to infer the neutral temperature of the rail; (4) the method works well if an accurate model of the dynamic response of CWRs to localized lateral forces is available.

ROADMAP FOR IMPLEMENTATION. This project set the ground for a new NDE method that can provide the necessary level of accuracy with minimum traffic disruption, and with a few measurements that do not require day-long observations under favorable weather, and without permanent wayside installations. The findings of this T-86 project validated all the research hypotheses behind the project and proved that the models are valid.

1. IDEA PRODUCT

Most modern railways are made of continuous welded rails (CWRs) that, when laid, are pre-tensioned to counteract the thermal expansion occurring in warm days. The typical state of stress at the moment of the anchorage is such that the rail neutral temperature (RNT) T_N, i.e. the temperature at which the net longitudinal force is zero, is comprised between 90°F and 110°F (32°C and 43°C). Thermal contraction or expansion due to air cooling or heating, respectively, cause hourly and seasonal variation of the axial stress along the rail. As such, RNT much higher than 110°F can result in very high tensile forces in cold weather increasing the likelihood of a broken rail, while RNT much lower than 90°F can result in very high compressive forces during hot weather, increasing the likelihood of buckling. The industry has found that laying and maintaining CWRs within a RNT range of 90 - 110°F is an effective compromise. Over the years the RNT decreases to unknown values increasing the risk of buckling. Buckling occurs when the temperature T_R of the rail steel reaches the critical temperature T_{cr}, which in turn is related to the buckling stress σ_{cr}, with the known formula:

$$\frac{\sigma_{cr}}{E\alpha} + T_N = T_{cr} \quad (1)$$

Here, E and α indicate the Young's modulus and the coefficient of thermal expansion of the rail steel, respectively. As σ_{cr}, E, and α are typically known, buckling may be prevented by estimating the temperature T_{cr} at which the rail will buckle. As Eq. (1) requires the accurate knowledge of the neutral temperature, there is a need for nondestructive evaluation (NDE) methods to measure T_N *in situ*, any time of the year. Alternatively, T_N can be inferred indirectly by measuring non-invasively the longitudinal stress σ_R at any temperature T_R, and then applying the equation:

$$T_N = T_R - \frac{\sigma_R}{E\alpha} \quad (2)$$

Rail stress is therefore a key parameter to guarantee safe operations and avoid rail buckles and pull-a-parts. The non-invasive estimation of rail stress may prevent derailments or slow orders. Current nondestructive evaluation (NDE) methods to estimate stress or infer the RNT have one or more shortcomings that limit widespread consensus. In this Type 1 Transit IDEA project, a NDE method based on the propagation of highly nonlinear solitary waves is proposed. The overall principle is illustrated with Fig. 1. An array of spherical particles (Fig. 1a) is in point-contact with the web of the rail to be evaluated. At one end of the chain, a single pulse, hereinafter referred to as the incident solitary wave (ISW), is generated for example by lifting and releasing the first bead in order to create a collision between the particle and the chain.

The ISW propagates along the array and when it reaches the opposite end of the chain that is in contact with the rail, part of its energy reflects back giving rise to a primary reflected solitary wave (PSW). Under certain circumstances a second pulse, hereinafter referred to as the secondary reflected solitary waves (SSW), arises. The SSW is observable when the ISW is strong enough or the rail is compliant enough to deform elastically the medium at the interface.

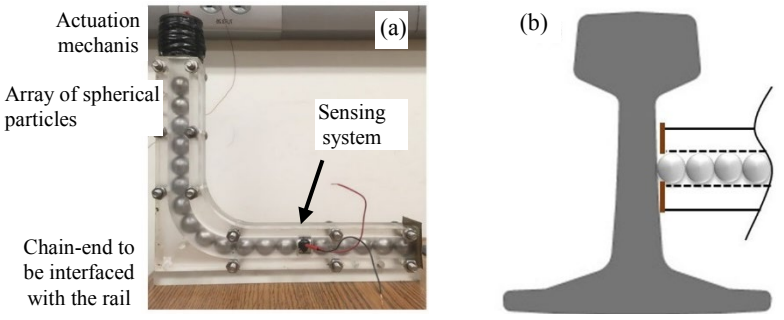

FIGURE 1 General principles of the proposed NDE method. (a) Photo of a *transducer* able to trigger, sustain, and detect the propagation of solitary waves. (b) Schematics of the point-contact between the *transducer* and a rail.

The high-risk high-innovation hypothesis investigated in this T-86 project is that the amplitude and time of flight of the reflected waves are dependent on the axial stress. The hypothesis leverages upon early works conducted by the principal investigator under a Federal Railroad Administration (FRA) grant. The summary of those findings is presented in Table 1.

TABLE 1 Findings of PI's Early Works that Support the High-Risk High-Innovation Hypothesis of this T-86 Project

Reference	**Main project outcome**
(Ni et al. 2013)	Proved experimentally that HNSWs can be measured by three different sensing mechanisms. This provides more flexibility in the design of the transducers.
(Cai et al. 2013a)	Proved numerically and experimentally that HNSWs can propagate along curved chains
(Cai et al. 2013b)	Proved that HNSWs propagating along straight chains are affected by the geometric and mechanical properties of slender thin beams in contact with the chain.
(Bagheri et al. 2015a)	Proved numerically that HNSWs propagating along straight chains are affected by the neutral temperature of slender beams in contact with the chain.
(Bagheri et al. 2015b)	Proved numerically and experimentally that HNSWs along L-shaped chains of particles are affected by thermal stress applied to slender beams.
(Bagheri et al. 2016a)	Optimized numerically the design of straight chains in order to maximize the sensitivity to thermal stress in slender beams.
(Bagheri et al. 2016b)	Proved numerically and experimentally that HNSWs propagating along straight chains of particles are affected by thermal stress applied to slender beams.

To investigate the high-risk high-innovation hypothesis and to evaluate the feasibility of the proposed method, the following **work plan** was executed:

(1) created models about the rail-chain interaction by considering three kinds of structures: thick beams, unconstrained rails, and rails constrained by lateral springs that mimic the effects of crossties.

(2) assembled and tested four different kinds of *transducer* in order to identify the most practical and cost-effective design. The term *transducer* indicates a "plug-and-play" device made of: (a) a chain of spheres able to support the propagation of solitary waves; (b) a trigger to excite the waves; (c) a sensor to measure the waves; (d) a frame to encase the three components.

(3) validated the models by testing a thick beam and two rails using the most practical and cost-effective *transducer*.

The project deliverables were the:

1) design of the optimal "plug-and-play" device;

2) creation of generalized models able to predict the effect of the rail longitudinal stress on selected features of the solitary waves;

3) validation of the models.

The original work breakdown of this T-86 project consisted of two stages and five tasks. The first stage was about the development of the plug-and-play device, whereas the second stage was about testing the research hypothesis using the developed plug-and-play device. During the project, new tasks were added in order to broaden the scope of the project and gain more knowledge about ***ANTEUSW***. The most important adds-on to this project were the numerical models and the test of a 2.4 m long rail. For the sake of completeness, the original scope of work is presented in what follows.

STAGE 1: Refine the Design of the plug-and-play device (Duration 6 months)

Stage 1, Task 1: Design the plug-and-play device

We consider and test two kinds of systems to excite the SWs within the chain. One is a mechanical striker, made of a particle identical to the beads forming the chain, driven by an electromagnet to trigger the propagation of a SW. The second system consists of a piezo-actuator in contact with one end of the chain. The unproven concept to be proved is that a piezo-actuator generates more repeatable waves. We assemble eight identical straight chains made of 19.05 mm steel particles and place them above the web of a rail laid, for practical purposes, on its side. Four chains are surmounted by an electromagnet to trigger a solitary pulse and the other four are surmounted by a piezo-stack actuator. Each chain embeds a thick disk sensor, which consists of a wafer-transducer glued between two thick disks. We drive the transducers with a National Instruments-PXI running in LabView in order to control the 8 transducers sequentially in a single experiment. The same tests is conducted using the L-shaped chains that are more practical for field applications.

Stage 1, Task 2: Stage I Report:

A Stage I draft report is prepared and submitted by the principal investigator to the expert panel. Following this review, a Stage 1 final report is submitted to the IDEA program office, along with written review comments and responses.

STAGE 2: Test the plug-and-play device on thick beams and short rail segments (Duration 12 months)

STAGE 2, Task 3: Test Thick Beams

We test a thick beam "similar" to an AREMA 141 cross-section. The similarity is such that thermal buckling occurs at temperature similar to those observed in real rails. The objective is two-fold: (1) prove that the technology can be applied to thick structures; (2) prove that the proposed NDE method is repeatable, reliable, and accurate.

Two of the four L-shaped transducers assembled and tested in Task 1 are used. We evaluate the two solutions discussed in section 1. For each experiment, the HNSW transducer is placed in contact with the mid-span of the thick beam held in tension and subject to thermal stress using a thermal tape. The waves are measured during the heating and the cooling ramp, and we plan to complete two heating-cooling cycles per day. For each experiment, we extrapolate one or more equations that link one or more features of the solitary waves to thermal stress.

The experiments is repeated by pre-tensioning the beam at 10%, 30%, and 50% of the material's yield. This mimics different neutral temperatures and mimics real rail scenarios where the RNT changes over time.

STAGE 2, Task 4: Test Rail Segments

We test the proposed NDE method against real rail sections donated to the PI's group a few years ago. We quantify the interaction between the chain and thermal stress. First, the rail is at rest and no load is applied. Then, the same rail is placed in a MTS machine operated in displacement control and driven such that no displacement is allowed. Simultaneously the rail will be heated using thermal tape and lamps, and periodically probed with the plug-and-play devices. The objective of the experiments is to demonstrate that the propagation of SWs is influenced by thermal stress. We anticipate that we will not be able to pretension the rail.

STAGE 2, Task 5: Draft Final Report and Final Report.

The principal investigator (PI) prepares and submits a draft final report documenting the project's results. The draft final report includes the results of all tasks. The draft final report is distributed to the Transit IDEA program manager and to the expert review panel for review and comments. The investigators will address the comments from the reviewers in a revised draft report and submit the report, along with written responses to review comments, to the IDEA program office.

This final report is organized as follows: Section 2 presents the finite element model and the discrete particle model developed to predict the sensitivity of the proposed NDE method to the variation of longitudinal stress in the rails. Section

3 describes the experiments conducted to evaluate the repeatability of the *transducers*, and is organized in three subsections: test setup; experimental results; comments and conclusions relative to this portion of the study. Section 4 presents the numerical and experimental studies about the thick beam and rails. This Section 4 is organized in four parts: beam testing; numerical analysis of rails; rail experiments; comments and conclusions relative to this portion of the study. Section 5 ends the report with some concluding remarks about the major outcomes of the project and explains how the method would be implemented in the field, i.e. it describes the practicality of the method. Section 6 elaborates the plans for implementation and describe the overall roadmap of the technology. Finally, section 7 describes the profile of the investigators.

2. CONCEPT AND INNOVATION

2.1 MODELS

The formulation of the models is pivotal to quantify the sensitivity of the proposed NDE method to variables such as the length, cross-section, and boundary conditions of the rail, as well as the longitudinal stress. Accurate models are necessary to take into account any (potential) effect of missing ties or missing fasteners in real rails.

A finite element model of the rail was combined with the discrete particles model of the chain using MATLAB®. The full formulation of both models was presented first in (Nasrollahi and Rizzo, 2018) where the interaction between a chain and a beam of thickness and height comparable to rail webs was described. Then, the models were improved and expanded to the case of rails (Nasrollahi and Rizzo, 2019). For the sake of completeness, a brief review of these models is given here.

A two-node beam element with two translational and one rotational degree of freedom at each node was considered. The local elastic stiffness matrix was (Zienkiewicz and Taylor, 2013):

$$\boldsymbol{K_E} = \begin{bmatrix} \frac{EA}{l_e} & 0 & 0 & -\frac{EA}{l_e} & 0 & 0 \\ 0 & \frac{12EI}{l_e^3} & \frac{6EI}{l^2} & 0 & -\frac{12EI}{l_e^3} & \frac{6EI}{l_e^2} \\ 0 & \frac{6EI}{l_e^2} & \frac{4EI}{l_e} & 0 & -\frac{6EI}{l_e^2} & \frac{2EI}{l_e} \\ -\frac{EA}{l_e} & 0 & 0 & \frac{EA}{l_e} & 0 & 0 \\ 0 & -\frac{12EI}{l_e^3} & -\frac{6EI}{l_e^2} & 0 & \frac{12EI}{l_e^3} & -\frac{6EI}{l_e^2} \\ 0 & \frac{6EI}{l_e^2} & \frac{2EI}{l_e} & 0 & -\frac{6EI}{l_e^2} & \frac{4EI}{l_e} \end{bmatrix} \tag{3}$$

where l_e represents the length of the single element. In presence of axial stress σ in the rail, the geometric stiffness matrix $\boldsymbol{K_G}$ of the element became (Zienkiewicz and Taylor, 2005):

$$\boldsymbol{K_G} = \frac{\sigma \cdot A}{l_e} \begin{bmatrix} 0 & 0 & 0 & 0 & 0 & 0 \\ 0 & \frac{6}{5} & \frac{l_e}{10} & 0 & -\frac{6}{5} & \frac{l_e}{10} \\ 0 & \frac{l_e}{10} & \frac{2l_e^2}{15} & 0 & -\frac{l_e}{10} & -\frac{l_e^2}{30} \\ 0 & 0 & 0 & 0 & 0 & 0 \\ 0 & -\frac{6}{5} & -\frac{l_e}{10} & 0 & \frac{6}{5} & -\frac{l_e}{10} \\ 0 & \frac{l_e}{10} & -\frac{l_e^2}{30} & 0 & -\frac{l_e}{10} & \frac{2l_e^2}{15} \end{bmatrix} \tag{4}$$

Here, σ is negative when the element is under compression. To account for the characteristics of the rail, the area A and the moment of inertia I of the rail section profile to be considered are substituted in the elastic and in the geometric matrixes. The stiffness matrix $\boldsymbol{K}$ of the element is the sum of the elastic and the geometric stiffness matrices, i.e:

$$\boldsymbol{K} = \boldsymbol{K_E} + \boldsymbol{K_G} \tag{5}$$

The local compatibility mass matrix of the structural element is instead:

$$\boldsymbol{M} = \rho \cdot A \cdot l_e \begin{bmatrix} \frac{1}{3} & 0 & 0 & \frac{1}{6} & 0 & 0 \\ 0 & \frac{13}{35} & \frac{11l_e}{210} & 0 & \frac{9}{70} & -\frac{13l_e}{420} \\ 0 & \frac{11l_e}{210} & \frac{l_e^2}{105} & 0 & -\frac{13l_e}{420} & -\frac{11l_e^2}{210} \\ \frac{1}{6} & 0 & 0 & \frac{1}{3} & 0 & 0 \\ 0 & \frac{9}{70} & -\frac{13l_e}{420} & 0 & \frac{13}{35} & -\frac{11l_e^2}{210} \\ 0 & -\frac{13l_e}{420} & -\frac{11l_e^2}{210} & 0 & -\frac{11l_e^2}{210} & \frac{l_e^2}{105} \end{bmatrix} \tag{6}$$

where ρ is the density of the rail steel.

Depending upon the length of the rail to be considered, the number of discrete elements may vary. After discretization, the local stiffness and the local mass matrices of each element, obtained using Eqs. (2)-(5), were transformed into the global coordinates and then assembled to form the global stiffness and mass matrices of the whole rail.

To account for the presence of the crossties, lateral springs were modeled using spring elements with stiffness matrix:

$$\boldsymbol{K_t} = \begin{bmatrix} k_t & -k_t \\ -k_t & k_t \end{bmatrix} \tag{7}$$

where k_t is the tie stiffness.

For the L-shaped granular medium shown in Fig. 1a, a 2-D discrete mass/spring model was implemented and the full formulation was also presented in (Nasrollahi and Rizzo, 2018). Here, each bead had two translational degrees of freedom, the masses were assumed concentrated at the center of the sphere, and a Hertzian contact was imposed acting along the line of sight between two adjacent particle centers (Nesterenko, 1983; 2001).

A finite element analysis of an axially loaded rail in contact with an L-shape HNSW transducer was formulated by coupling the meshed rail to the discrete model of the chain particles.

2.2 TRANSDUCERS DESIGN AND VALIDATION

The design of the *transducers*, is pivotal to the successful measurement of the stress, as the *transducer* is the "plug-and-play" device to be used to inspect the rail. In addition, any *transducer*-to-*transducer* difference resulting from the assembly of the device components may reduce the ability to estimate the stress accurately. A *transducer* consists of five parts: 1) a finite number of spheres; 2) a frame holding the particles; 3) an actuation mechanism able to trigger the solitary pulses; 4) a sensing system able to measure the waves propagating within the chain; 5) a thin sheet glued at the opposing end of the frame to prevent the free fall of the particles. A single data acquisition system controls the *transducer* and store the signals for post-processing analysis.

Four different designs were considered, namely an L-shaped and a straight shaped frame and, for each frame, two actuation mechanisms were considered: an electromagnet and a mechanical shaker. A photo of one L-shaped device with an electromagnet on top is shown in Fig. 1a; a straight *transducer* with an electromagnet is shown in Fig. 2. For each frame

shape, four *transducers* were assembled and tested in order to quantify *transducer*-to-*transducer* differences and the repeatability of the propagating pulses. All transducers contained 19.05 mm in diameter stainless steel particles with the exception of the second particle from the top that was non-ferromagnetic for reasons that will be explained later. The sensing system consisted of a 19.05 mm diameter piezoelectric (PZT) element embedded between two 6.05 mm thick disks of 19.05 mm diameter.

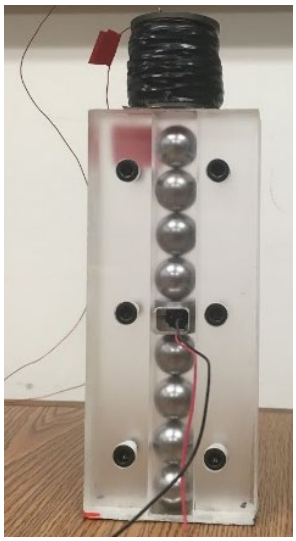

FIGURE 2 Photo of a straight *transducer*. Not visible here, a 0.25 mm thick aluminum foil is glued at the bottom of the frame to prevent the free fall of the beads.

The two actuation mechanisms were an electromagnet built in the lab and connected to a commercial DC power supply to lift and release the first particle of the chain, and a commercial shaker (LDS V201), connected to a dedicated amplifier. The shaker mounted a long screw to which a hemispherical bead was glued. With this arrangement, the electronic control of the shaker tunes the collision of the hemi-bead with the chain. In fact, the collision force can be increased/decreased by increasing/decreasing the output of the amplifier. With respect to the first actuation mechanism, the shaker provides better control of the collision force at the expense, though, of a bulkier and more expensive overall system. In addition, while the previous arrangement can be used and was used to drive many transducers simultaneously, the amplifier can be connected to one shaker only. All *transducers* were connected to and driven by a National Instruments-PXI 1042Q running in LabVIEW. Two graphical user interfaces were created, one for each kind of actuation mechanism. For the shaker-based transducer, the PXI controlled a LDS PA25E linear amplifier (Fig. 3a) that was, in turn, connected to a LDS V201. The shaker was mounted above the chain as shown in Fig. 3b.

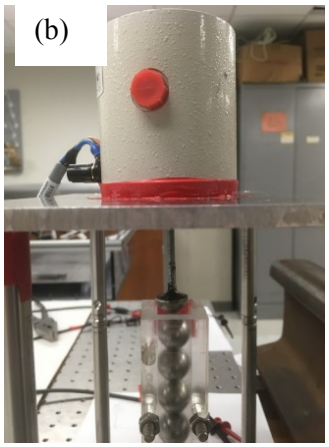

FIGURE 3 (a) LDS PA25E amplifier used to drive the shaker (b) Close-up view of the shaker mounted above the chain of particles. A half-particle, screwed to the shaker, generates the impact necessary to trigger the ISW.

3. INVESTIGATION

3.1 TRANSDUCERS TESTING: SETUP

Four straight and four L-shaped chains were assembled and tested. Time-wise, the sequence of the experiment was the following. First, four electromagnets were glued to the four straight chains and tested simultaneously (Fig. 4a). Then, the same electromagnets were glued to the four L-shaped chains (Fig. 4b) that were then tested simultaneously. Five hundred measurements were taken from each *transducer* and the signals were sampled at 1 MHz. The falling height of the striker was about 4 mm. At last, the shaker was mounted to every chain. Owing to the ability to drive one shaker at the time, eight experiments were run separately. Here, the sampling frequency was also 1 MHz. The amplitude of the incident wave was controlled with the amplifier. Five hundred measurements were taken as well.

To examine the effect of the impact force on the repeatability of the solitary waves, two rounds of experiments were conducted twice: one using a low input force able to produce a +3V pulse amplitude, and one using a high impact (+5V amplitude). Based on all the above, 10,000 waveforms were analyzed processed. The transducers were in contact with the web of a 0.72 m long AREMA rail. To test the straight transducers, the rail was rotated by 90º along its longitudinal axis.

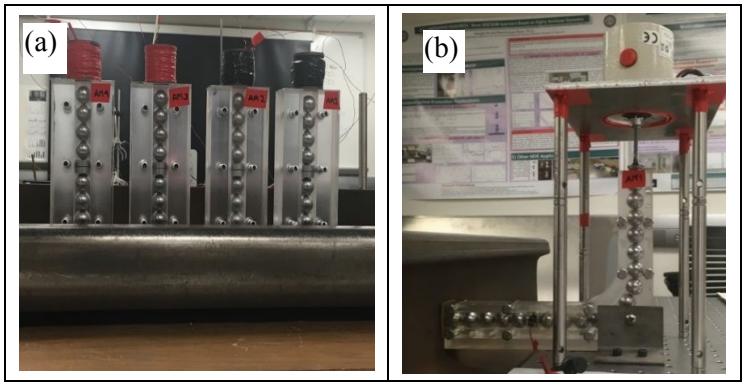

FIGURE 4 (a) Photo of the four straight *transducers*, each driven with an electromagnet. The *transducers* are located above the web of a short rail segment which was flipped for practical purposes. (b) Photo of one of the L-shape *transducers* driven with the shaker in contact with the web of the rail. The transducer was fixed to an optical table to prevent any horizontal movement.

3.2 TRANSDUCERS TESTING:RESULTS

Figure 5 exemplifies the typical shape of the incident and the primary reflected pulse. The amplitude of the incident wave, the ratio of the amplitude of the PSW reflected at the chain-rail interface to the amplitude of the ISW, and the time-of-flight (TOF) were the wave features examined to quantify the repeatability of the *transducers*.

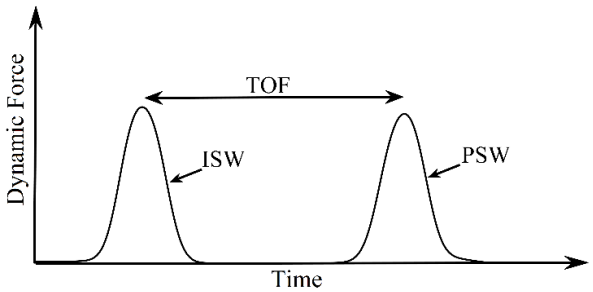

FIGURE 5 Typical solitary wave pulses detected when the transducers were in contact with the short rail. The first pulse is the incident solitary pulse; the later pulse is the wave reflected at the chain-rail interface. The time of flight (TOF) is the difference in the arrival time of the maximum amplitude of the two waves at the same sensing location. The amplitude of the two pulses is used to calculate the ratio between the PSW to the ISW.

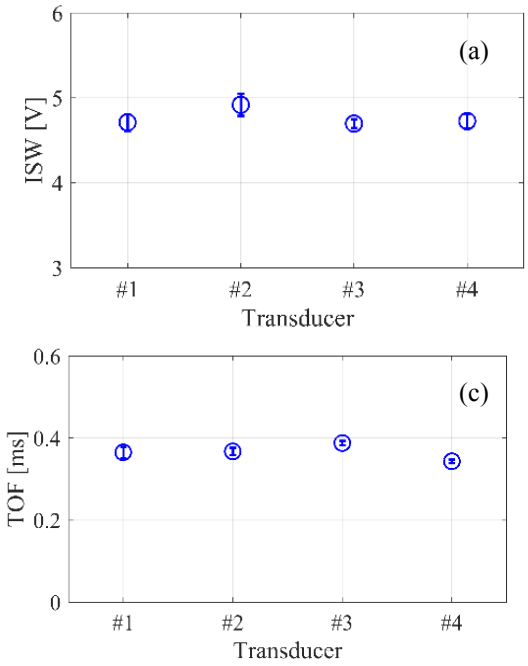

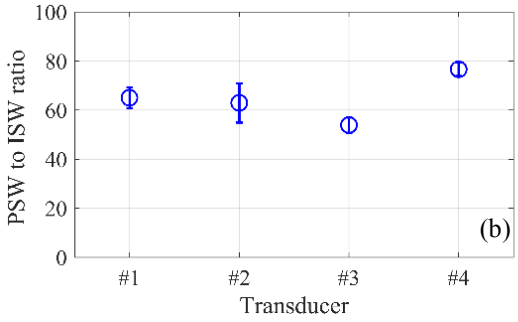

FIGURE 6 Mean value and standard deviation of the solitary wave features extracted from the time waveforms measured in the straight *transducers* driven with an electromagnet. (a) Amplitude of the ISW, (b) PSW to ISW amplitudes ratio expressed in percent, and (c) TOF.

TABLE 2 The Statistical Parameters Of The Solitary Wave Features Extracted From The Time Waveforms Measured In The Straight Transducers Driven With An Electromagnet.

Transducer	ISW (V)			PSW/ ISW (%)			TOF (ms)		
	Mean	SD	CoV (%)	Mean	SD	CoV (%)	Mean	SD	CoV (%)
#1	4.711	0.099	2.10	65	4	6.15	0.3650	0.0138	3.78
#2	4.918	0.130	2.64	63	8	12.7	0.3674	0.0087	2.37
#3	4.798	0.050	1.04	54	3	5.56	0.3878	0.0052	1.34
#4	4.726	0.088	1.86	77	3	3.90	0.3433	0.0043	1.25

SD: Standard Deviation; CoV: Coefficient of Variation

Figure 6 presents the average value (out of the 500 measurements) of the three features associated with the straight *transducers* activated with the electromagnet. For each value, the vertical bars are twice the corresponding standard deviation (SD). For convenience, the results are also presented in Table 2, which includes the coefficient of variation (CoV) that is the ratio of the standard deviation (SD) to the corresponding mean value. The results shown in Fig. 6 and summarized in Table 2 demonstrate that:

1) The amplitude of the pulses generated with the same *transducer* is highly repeatable given that the corresponding CoV is between 1.0% (*Transducer* #3) and 2.6% (*Transducer* #2). The average amplitude of the ISW across the *transducers* is 4.79 V and the corresponding CoV is 1.8%. This suggests that the proposed design induces little *transducer-to-transducer* difference at least in terms of the amplitude of the incident signal.
2) The feature of the PSW-to-ISW ratio is not as repeatable as the amplitude of the incident wave. The CoV relative to a given device ranges between 3.9% (*Transducer* #4) and 12.7% (*Transducer* #2) whereas the CoV among the four transducers is about 12.7%. It is noted here that the surface of the rail was slightly sandblasted. It is believed that the difference across the four transducers arises from small variations in the chain alignment inside the frame, friction between the spheres and the inner wall of the frame, and unplanned rotation of the sensor disks during the experiment. Still, the repeatability within each transducer is very high, given that they were assembled manually.

3) The ToF is a better feature than the amplitude-based feature. The CoV within the same transducer ranges from 1.3% and 3.8% whereas the same coefficient measured across the four transducers is equal to 4.3%. The result suggests that the TOF is the main candidate to consider for the evaluation of the axial stress along thermally loaded rails.

A similar analysis was carried for the four L-shaped transducers driven with an electromagnet and the results are summarized in Table 3. When compared to the corresponding values of the straight chains, it is noted that the CoVs are overall higher than the their counterpart in Table 2.

TABLE 3 The Statistical Parameters of the Solitary Wave Features Extracted from the Time Waveforms Measured in the L-Shaped Transducers Driven with an Electromagnet.

Transducer	ISW (V)			PSW/ ISW (%)			TOF (ms)		
	Mean	SD	CoV (%)	Mean	SD	CoV (%)	Mean	SD	CoV (%)
#1	2.669	0.036	1.4	96	11	11.2	0.4354	0.0067	1.5
#2	2.144	0.126	5.9	81	8	10.8	0.4409	0.0264	6.1
#3	2.808	0.062	2.2	78	5	6.4	0.4549	0.0129	3.0
#4	2.871	0.070	2.4	82	7	8.3	0.4419	0.0122	2.8

To ease the comparison between the two geometries driven with an electromagnet, Table 4 contains the average, the SD and the CoV of the two designs. The amplitude of the ISW in the L-shaped chain is smaller and less repeatable than the straight chain. This is due to signal attenuation along the elbow and the horizontal leg of the frame due to friction between the spheres and the inner wall. On the contrary, the PSW/ISW ratio and the TOF are more repeatable among the L-shaped *transducers* because the sensor disk, owing to its location along the horizontal leg of the frame, is less prone to misalignment. The results presented in Tables 2-4 suggest that the L-shaped *transducer* should be preferred to the straight one because it is easier to deploy in real railroad tracks and provides more repeatable measurements.

TABLE 4 Statistics Associated with the Straight and the L-Shaped Transducers, Both Driven by an Electromagnet.

Transducer	ISW (V)			PSW/ ISW (%)			TOF (ms)		
	Mean	SD	CoV (%)	Mean	SD	CoV (%)	Mean	SD	CoV (%)
Straight	4.788	0.082	1.71	64.75	8.2	12.7	0.366	0.016	4.31
L-shaped	2.623	0.286	10.9	84.25	6.9	8.2	0.443	0.007	1.61

The results relative to the shaker-based actuator are presented in Tables 5 and 6. Table 5 summarizes the features relative to the straight *transducers*. The columns of the coefficient of variation show smaller variability with respect to the electromagnetic-driven *transducers* (Table 2), implying that the solitary wave features are more repeatable when the ISW is triggered with the shaker.

TABLE 5 The Statistical Parameters of the Solitary Wave Features Extracted from the Time Waveforms Measured in the Straight Transducers Driven with a Shaker.

Transducer	ISW (V)			PSW/ ISW (%)			TOF (ms)		
	Mean	SD	CoV (%)	Mean	SD	CoV (%)	Mean	SD	CoV (%)
#1	5.115	0.037	0.7	68	4	5.9	0.3657	0.0067	1.8
#2	5.165	0.073	1.4	71	2	2.8	0.3681	0.0041	1.1
#3	5.113	0.046	0.9	52	3	6.2	0.3885	0.0027	0.7
#4	5.144	0.083	1.6	66	4	6.1	0.3439	0.0022	0.6

The CoVs of the TOF are nearly half the electromagnetic actuation case. The one-to-one comparison between the shaker-driven and the electromagnet-driven *transducers*, i.e. between Table 5 and Table 2, demonstrate that:

1) The ISW is higher in the shaker-driven *transducer* because of the stronger collisions produced by the shaker.

2) The CoV of all features is smaller in the shaker-driven *transducer* likely because it is electronically controlled.

3) The PSW/ISW is more consistent in the shaker suggesting that this feature might be a function of other parameters such as the surface condition, the internal friction, etc.

The results of the L-shaped *transducer* activated with a shaker are presented in Fig. 7 and Table 6. Two rounds of experiments were carried out. In one round, the gain of the amplifier was set such that the amplitude of the ISW was equal to ~5 V. In the second round, the gain trigger ISW amplitudes in the order of 3V. These two sets of experiments enabled to consider any effect of the actuation force on the features of the propagating waves.

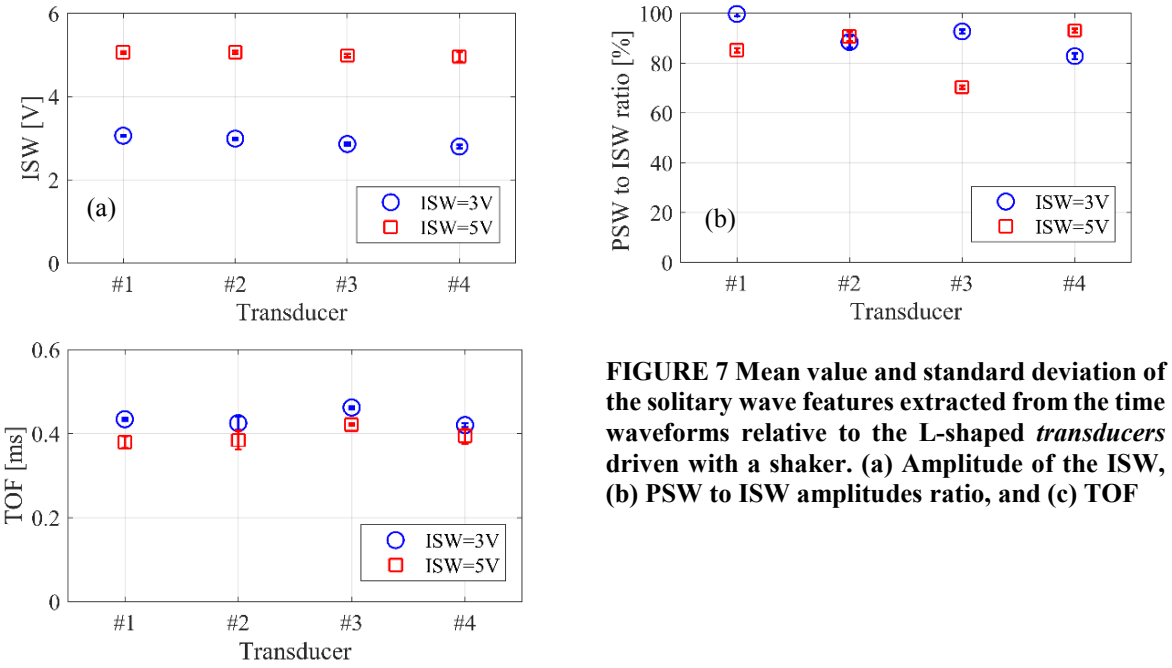

FIGURE 7 Mean value and standard deviation of the solitary wave features extracted from the time waveforms relative to the L-shaped *transducers* driven with a shaker. (a) Amplitude of the ISW, (b) PSW to ISW amplitudes ratio, and (c) TOF

In the figure, the values of both experiments are overlapped on the same subplots. **Figure 7b** shows that the PSW/ISW ratio was not proportional to the amount of acoustic energy induced in the grains. Still, the experiments were highly repeatable and the coefficients of variation associated with each set of 500 measurements were between 0.8% and 2.6%. The TOF (Fig. 7c) was instead inversely proportional to the amplitude of the ISW. This result was expected as one of the peculiar properties of the solitary waves is that the wave's dynamic force and speed are directly proportional. The consequence is that the time of flight of the solitary waves is smaller for faster waves, i.e. for higher amplitude waves as visible in Fig. 7c. When compared to Table 2, the results presented in Table 5 suggest that the shaker provides more repeatable results.

TABLE 6 The Statistical Parameters of the Solitary Wave Features Extracted from the Time Waveforms Measured in the L-Shaped Transducers Driven with a Shaker.

Transducer	ISW (V)			PSW/ ISW (%)			TOF (ms)		
	Mean	SD	CoV (%)	Mean	SD	CoV (%)	Mean	SD	CoV (%)
	ISW = 5 V								
#1	5.062	0.029	0.5	85	4	1.0	0.3798	0.0147	3.9
#2	5.068	0.036	0.7	90	9	2.0	0.3847	0.0220	5.7
#3	4.985	0.041	0.8	70	3	0.9	0.4216	0.0028	0.7

#4	4.963	0.117	2.3	93	3	0.8	0.3938	0.0173	4.4

Transducer	**ISW = 3 V**								
#1	3.060	0.014	0.5	100	5	0.9	0.4339	0.0030	0.7
#2	2.991	0.023	0.8	88	12	2.6	0.4248	0.0164	3.9
#3	2.863	0.033	1.2	93	4	0.9	0.4618	0.0027	0.6
#4	2.802	0.045	1.6	83	6	1.4	0.4200	0.0049	1.2

3.3 DISCUSSION AND RECOMMENDATION ABOUT TRANSDUCER DESIGN

Four *transducer* designs were considered, assembled, and tested to quantify their repeatability in terms of pulse excitation and detection. Five sets of experiments were conducted using the same experimental protocol. Table 7 compares the results of these five sets, by showing the average value of the three most relevant wave characteristics for each design. The CoV is the metric that was used to quantify the *transducer* repeatability. The coefficient relative to the incident pulse is below 3.5% for all cases except the L-shaped *transducer* with an electromagnet, and the reason is that *Transducer* #2 was an outlier. The highest CoV relative to the TOF was 4.3% (straight *transducer* with an electromagnet).

TABLE 7 The Statistical Analysis of Different Transducers

***Transducer* Type**	**ISW (V)**			**PSW/ISW (%)**			**TOF (ms)**		
	Mean	**SD**	**CoV (%)**	**Mean**	**SD**	**CoV (%)**	**Mean**	**SD**	**CoV (%)**
Straight EM	4.788	0.082	1.7	65	8	12.7	0.3659	0.0158	4.3
L-shaped EM	2.623	0.286	10.9	84	7	8.2	0.4433	0.0072	1.6
Straight Shaker	5.150	0.028	0.5	69	6	8.7	0.3666	0.0068	1.3
L-shaped Shaker(5V)	5.020	0.046	0.9	85	9	10.5	0.3950	0.0162	4.1
L-shaped Shaker(3V)	2.929	0.102	3.5	91	6	6.9	0.4351	0.0162	3.7

Based on the above, advantages and limitations of each design are summarized in Table 8. Following the analysis of the advantages and limitations, it was determined that the L-shaped *transducer* driven with an electromagnet represents the best trade-off in terms of practicality, cost, and repeatability.

TABLE 8 Pros and Cons of the Four Kind of Transducers Considered in This Study.

***Transducer* Type**	**Advantages**	**Limitations**
Straight with EM	Lightest, cheapest, easiest to assemble with respect to the shaker-based actuator. Many *transducers* can be driven sequentially.	Collision forces cannot be varied. Challenging deployment when needed to be placed in contact to the web of a real rail.
L-shaped with EM	Lighter, cheaper, and easier to assemble with respect to the shaker-based actuator. Easiest to deploy when needed to be placed in contact to the web of a real rail. Many *transducers* can be driven sequentially.	Collision forces cannot be varied. Least repeatability (with respect to the other three designs).
Straight with shaker	Most repeatable pulses.	Heavier, more expensive, and more difficult to assemble with respect to the EM-based actuator. Challenging deployment when needed to be placed in contact to the web of a real rail. Only one transducer at the time can be driven.
L-shaped with shaker	Repeatable pulses. Easier (with respect to the straight shaker) to deploy when needed to be placed in contact to the web of a real rail.	Heaviest, most expensive, and most difficult to assemble with respect to the EM-based actuator. Only one transducer at the time can be driven.

3.4 BEAM TESTING

This section presents the numerical and experimental results of the beam rail testing. Following the recommendation provided in the previous section, one of the L-shaped *transducers* actuated with an electromagnet was used for the experiments. Table 9 lists the structures considered during this portion of the study. The cross-section of the beam was close to the size of a rail web; the rail profile was chosen to be identical to the profile of the rails available in the laboratory.

Table 9. Summary of the Structures Analyzed in this Project. For the Rail the Same AREMA $6^{13/16}$ was Used.

Structure	Numerical analysis	Experimental validation	Notes
Thick beam 1.2 m long	Yes	Yes	Mechanical and thermal loading
AREMA Rail 0.9 m long	Yes	Yes	Mechanical loading. The rail is modeled as an equivalent beam according existing studies presented in the scientific literature
AREMA Rail 2.4 m long	Yes	Yes	Same as above
AREMA Rail 3.6 m long	Yes	No	The rail is modeled as an equivalent beam according existing studies presented in the scientific literature
AREMA Rail 3.6 m long constrained with lateral springs	Yes	No	The rail is modeled as an equivalent beam according existing studies presented in the scientific literature. The stiffness of the rails is in agreement with what found in the literature.
AREMA Rail 4.8 m long	Yes	No	Same as above

A 0.127×0.016×1.4 m^3 A36 steel beam was connected to a MTS machine using two angled wedges at each end. The L-shaped *Transducer* #1 was placed in contact with the mid-span of the beam according to the setup visible in Fig. 8. The geometric and mechanical properties of the beam are listed in Table 10.

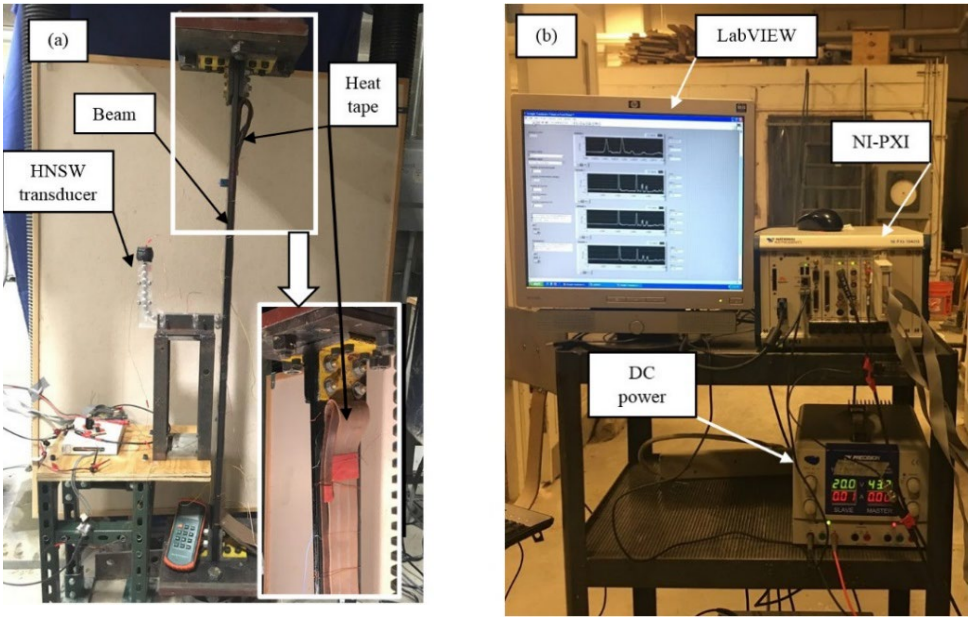

FIGURE 8 Beam testing: (a) photo of the beam and of the *transducer* including a close-up view of the anchoring system and of the thermal tape used to induce thermal stress; (b) hardware used to drive the *transducer*.

Table 10. Geometric and Mechanical Properties of the Thick Beam Tested in this Study.

w (mm)	h (mm)	L (mm)	E (GPa)	σ_y (MPa)	α (1/°C)	k	ρ (kg/m^3)
127	15.875	1400	205	250	1.0E-05	0.5	7850
I (mm^4)	A (mm^2)	r (mm)	λ	P_{cr} (kN)	σ_{cr} (MPa)	ΔT (°C)	m (kg)
42341	2016	5	131	238	118	48	19

w: width, h: depth, L: free length, α: coefficient of thermal expansion, k: buckling length ratio, ρ: density, r: radius of gyration, λ: slenderness

Mechanical and thermal load was applied to the beam according to the description of Table 11. In the mechanical testing, not presented here but reported in Nasrollahi and Rizzo (2018), the beam was mechanically loaded to its 25% of the tensile yielding stress. Then, the load was changed with -11 MPa steps to reach the beam's 25% buckling stress. At each step, ten measurements were taken with the *transducer*. Three tension-compression cycles were completed.

Table 11. Loading Protocol and some Details about the Four Experiments Performed with the Thick Beam.

Test No.	1	2	3	4
Load Type	Mechanical	Thermal	Thermal	Thermal
Pre-tension stress (MPa)	62.5	62.5	37.5	12.5
Yielding stress (%)	25	25	15	5
Compressive stress (MPa)	-30	-6	-18	-30
Buckling stress (%)	25	5	15	25
$\Delta\sigma$ (MPa)	92.5	68.5	55.5	42.5
Neutral temperature (°C)	25	25	15	5
Number of wave measurements at each step	10	5	5	5
Completed cycles	3	2	2	2

In the thermal testing, Tests No. 2,3, and 4 in Table 11, the specimen was pre-tensioned, held in displacement control, and then heated with a thermal tape to induce thermal stress. Three experiments were conducted corresponding to three levels of pre-tension, namely 25%, 15%, and 5% of the steel yielding stress. This mimicked different neutral temperatures. Heat was imparted until the surface temperature of the steel was about 82.5ºC, 71.6 ºC, and 63.3 ºC, respectively. Then, the beam was cooled naturally until the initial temperature was reached. By assuming fixed-fixed boundary conditions, the buckling load P_{cr} was estimated as:

$$P_{cr} = \frac{4\pi^2 EI}{L^2} \quad (7).$$

and the corresponding values for the test specimens are presented in Table 11.

A digital thermocouple was used to measure the temperature at the center of the beam, and five measurements were taken with the *transducer* at 5°C temperature step. At each step, the axial load shown in the MTS control box was recorded as well. Two cycles were completed for each test.

To quantify the feature gradient with respect to the axial stress the data points relative to the two heating and cooling ramps at any given stress were averaged and the results are presented in Fig. 9, overlapped to the numerical results of the finite element model. The equations of the line interpolation are presented as well and several conclusions can be drawn.

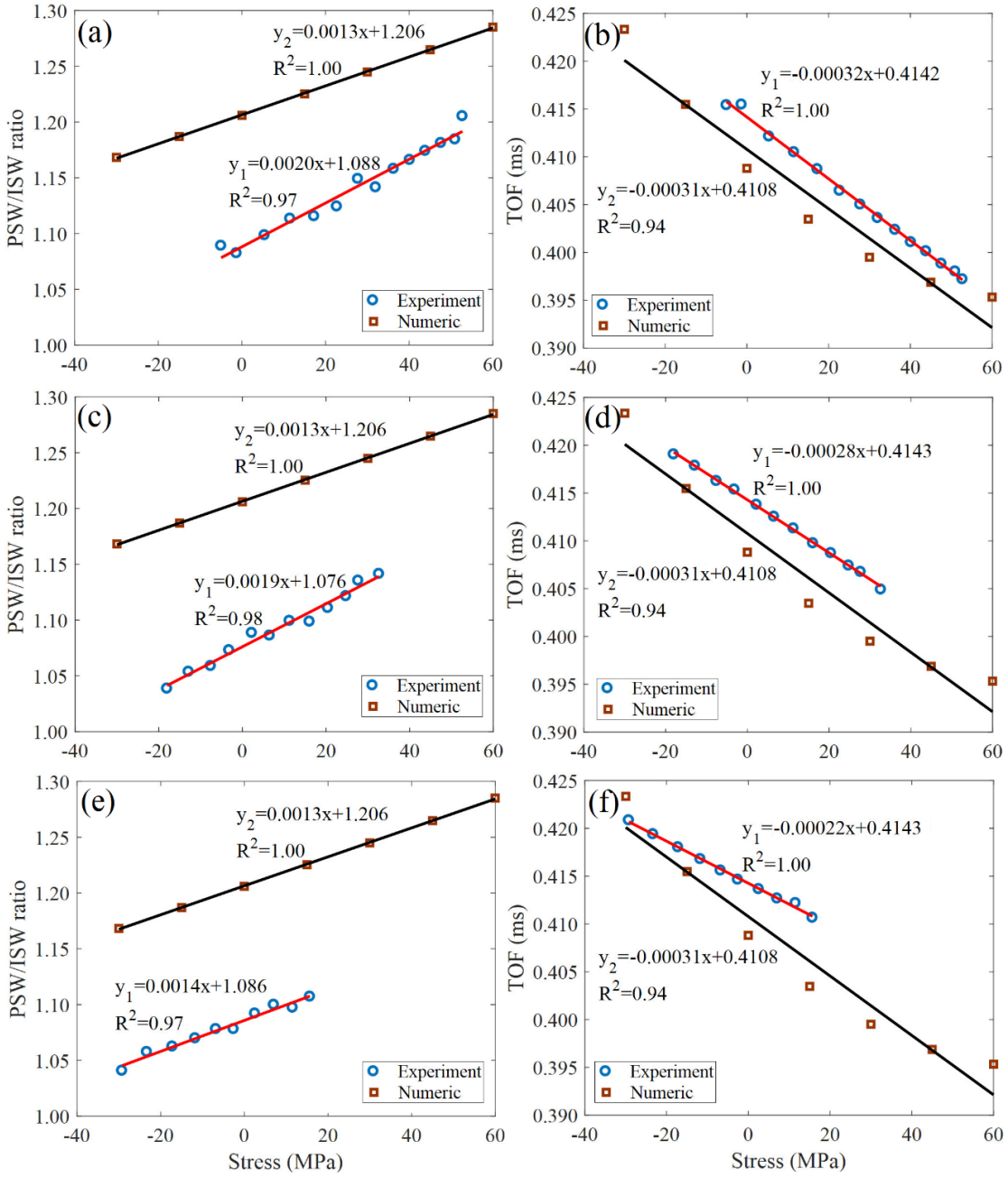

FIGURE 9 Experimental results of the thermal loading tests. Thermal loading tests, experimental results. Analysis of the features' trend: (a) PSW/ISW ratio and (b) TOF across [0.05σ_{cr}, 0.25σ_Y]; (c) PSW/ISW ratio and (d) TOF across [0.15σ_{cr}, 0.15σ_Y]; (e) PSW/ISW ratio and (f) TOF across [0.25σ_{cr}, 0.05σ_Y]. The results are fitted with linear interpolation and overlapped with the numerical predictions obtained using the finite element algorithm implemented in this project.

With the exception of Fig. 9(f), the slopes of the numerical and the experimental data are nearly identical. This means that the experimental slopes agree with the numerical prediction in terms of the sensitivity of the wave feature to the change in axial stress. The equations also reveal that the neutral temperature does not affect the sensitivity of the wave-based NDE method as the *y*-intercept does not change with the level of pre-tension: at zero stress, irrespective of the neutral temperature, the amplitude ratio is about 1.08 (108%) and the TOF is 0.414 ms. This implies that the method can be applied anytime regardless of the neutral temperature. In the field, the transducer would probe any thick beam with identical

geometric properties. The empirical TOF or amplitude ratio would be plugged into the y variable of the above equations to solve for the x variable, which represents the actual stress (σ_T). By measuring with a thermocouple the actual temperature T_f of the steel, the following equation:

$$\sigma_T = E\alpha\Delta T = E\alpha\left(T_0 - T_f\right) \tag{8}$$

would be used to infer the beam's neutral temperature. The possibility to use two wave features increases the redundancy of the proposed NDE system. The mismatch between numerical and experimental results is attributed to some inaccuracies in the parameters used in the model and to the grips holding the beam that did not realize the boundary conditions hypothesized in the model. Nevertheless, it can be concluded that, provided a model is available, axial stress can be determined and the neutral temperature of the beam has no influence on the sensitivity of the method.

3.5 RAIL TESTING

In the last three decades, many predictive models were developed to describe the buckling of CWRs. Most of them were finite element models in which the railroad track is considered "equivalent" to a single beam of finite length or to two parallel beams of finite length connected by lateral linear springs. The springs account for the tie-ballast stiffness. Irrespective of the number (one or two) of "equivalent" beams, the end supports are considered fixed.

Based on the works reported in the scientific literature, in this study the rail was modeled as an "equivalent" single beam. The effect of the axial stress was included in the $\boldsymbol{K_G}$ matrix (Eq. 4) whereas the use of the geometric nonlinear matrix ensures that buckling involves the whole length of the beam without the need for initial imperfection and without the need for computing large-deformation nonlinear analysis. Five AREMA rails of four different lengths were considered (Table 9). The elastic modulus of the rail steel was assumed 200 GPa, while the cross-sectional area and the moment of inertia were $8.74*10^{-3}$ m^2 and 7.04×10^{-6} m^4, respectively. The analysis of the shortest lengths (0.9 m and 2.4 m) was carried out to be able to validate experimentally the numerical predictions; as such this analysis was instrumental at proof the validity and the accuracy of the models. The longest (3.6 m and 4.8 m) rails were analyzed because their lengths are more consistent with what found in the scientific literature. The 3.6 m long rail was also constrained by lateral springs spaced 0.45 m apart. The stiffness k_t of the spring was set to 2.6×10^7 N/m, in accordance to (Lim et al. 2008). This analysis was performed to evaluate the effect of the crossties and lateral restrains on the features of the solitary wave. For consistency, the granular medium was identical to the L-shaped array tested earlier in the study.

Figure 10 shows the waveforms associated with two unconstrained rails, namely the 3.6 m long (Fig. 10a) and the 0.9 m long (Fig. 10b). The plots reveals the existence of the SSW in the longer rail whereas the short rail is too stiff to originate such a reflection. The presence of the SSW implies that the acoustic energy carried by the incident wave was sufficient to trigger a local oscillation of the structure and induced the separation of the bead from the rail. Interestingly, Fig. 10b reveals that the amplitude of the reflected pulse is higher than the amplitude of the incident wave. This apparent counterintuitive result is justified by the geometry of the transducer and by the power-law dependence of the phase velocity on the force amplitude, as fully detailed in Nasrollahi and Rizzo (2019).

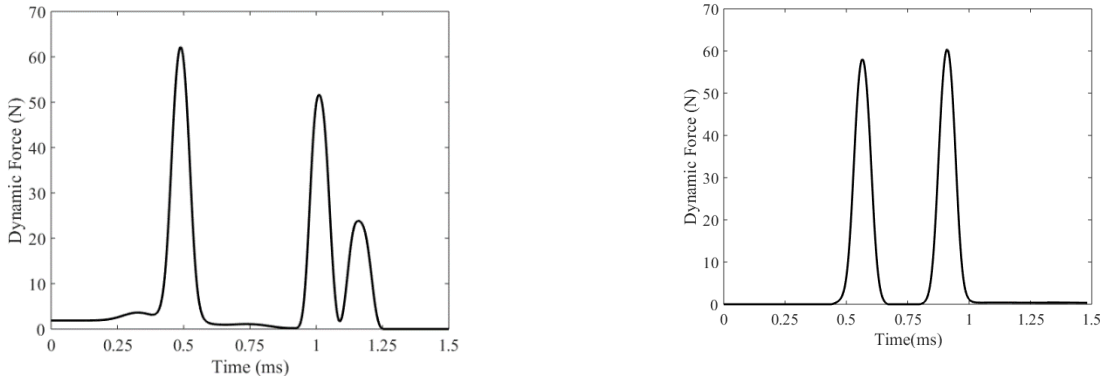

FIGURE 10 Numerical waveforms relative to the 3.6 m rail (left) and 0.9 m rail (right). The absence of a secondary pulse in the stiffer (shorter) rail is evident.

To investigate the influence of the axial stress on the characteristics of the waves reflected at the *transducer*-rail interface, some features of the reflected waves were computed for different values of longitudinal stress of the rail. The results relative to the four lenghts are presented in Fig. 11.

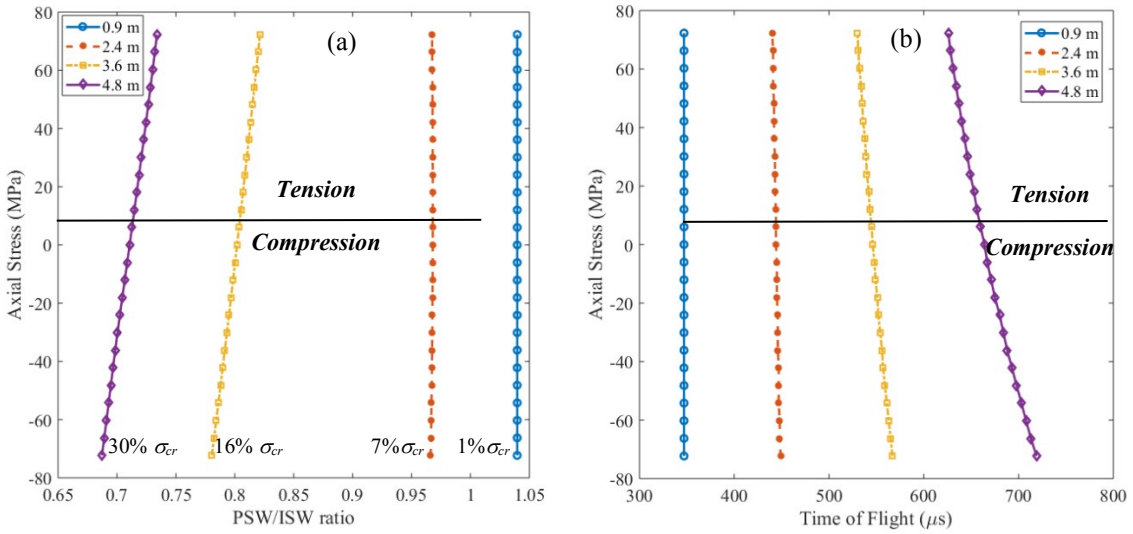

σ =3055*(ratio) - 2171
R^2=0.9998

σ=0.006326*TOF^2 - 10.04*TOF + 3874
R^2=0.9998

FIGURE 11 Numerical results. Axial stress as a function of two features of the solitary waves.

Figure 11a shows the axial stress (in the vertical axis) as a function of the amplitude ratio associated with the primary reflected wave for the four unconstrianed rails. Positive values refer to tensile stress. Here the analysis was conducted up to 11 ksi, equivalent to 17% of the yielding stress σ_Y, which is the same for any given length of the rail. In compression the stress of -11 ksi corresponds to different fraction of the buckling stress σ_{cr}, as shown in Fig. 11a. The figure shows that as the length of the "equivalent" beam increases, the feature of the primary reflected wave changes monotonically and an analytical relationship between the feature and the stress can be extracted. Such relationship is shown in Fig. 11a for the 4.8 m rail. Another interesting outcome of Fig. 11a is that within the stresses considered, any value of the feature is associated with only one curve. In other words, if the model accurately depicts real rails, the feature of the solitary wave would univocally determine the axial stress. However, the curves plotted in Fig. 11a have two variables: the stress and the

equivalent length. As such, another feature at least is necessary to solve for the stress. The other feature is shown in Fig. 11b in which the longitudinal stress is plotted as a function of the time of flight. This feature is also monotonically dependent to the stress and such sensitivity (slope of the curve) increases with the increase of the equivalent length. For convenience the equation of the polynomial interpolating the numerical findings is presented for the 4.8 m rail. The two polynomials displayed in Fig. 11 constitute the two (uncoupled) equations necessary to solve for the two variables of the problem: the "equivalent length" of the rail and the axial stress. The first variable is affected by the boundary conditions of the track, i.e. lateral resistance provided by the cross-ties and ballast, missing fasteners, etc.; the second variable depends on the actual temperature of the rail and the RNT. If other variables would appear in the problem, other wave features and therefore more polynomials may be considered.

In practice, the general finite element formulation would be adopted and adapted to the specific profile of the track to be inspected. By plugging the known mechanical and geometric properties of the rail in the finite element model, plots like those shown in Fig. 11 would be generated. In the field, the temperature T_R of the rail and the time waveforms such as those shown in Fig. 10 would be measured. From the waveforms, the PSW/ISW and the TOF would be extracted to identify the length of the equivalent beam and to infer the current stress σ_R in the rail (using one of the polynomials). The fact that all plots present a monotonic trend, guarantees that the solitary waves readings provide a unique value of the axial stress. With the estimated stress σ_R and the temperature T_R , the neutral temperature would be estimated using Eq. (2).

Besides the practical implications discussed with Fig. 11, some other considerations can be drawn from the analysis of Figs. 10 and 11. The shortest rail (0.9 m) is too stiff to induce any secondary reflection. Fig. 11a reveals that the amplitude of the reflected wave is about 4% higher than the incident wave (ration equal to 1.04). As said earlier, this finding is justified with the geometry of the L-shaped granular medium and the physical explanation was fully elaborated in Nasrollahi and Rizzo (2019). Finally, the length of the 0.9 m and 2.4 m rails is such that the rail would yield before buckling. As this scenario was, to the best of the investigators' knowledge, never observed in the field, these two rails were analyzed only to validate experimentally the numerical models.

The analysis with the lateral springs provided results very similar to those presented in Fig. 11, these results are therefore not presented here for the sake of space.

The 0.9 m long rail was mounted vertically in an MTS machine. The L-shaped *transducer* was placed in contact with the web at the midspan. Figure 12 shows the overall experimental setup. Mechanical compression was applied at 44.5 kN (10 kips) increments up to 445 kN (100 kips), which was about 20% of the critical load. Two load-unload cycles were completed. The load was recorded with the MTS control box. At the end of each load increment, ten measurements were taken with the *transducer*. The waveforms were sampled at 4 MHz and stored for post-processing analysis in which the amplitude of the incident wave, the PSW/ISW ratio, and the time of flight of the reflected wave were extracted.

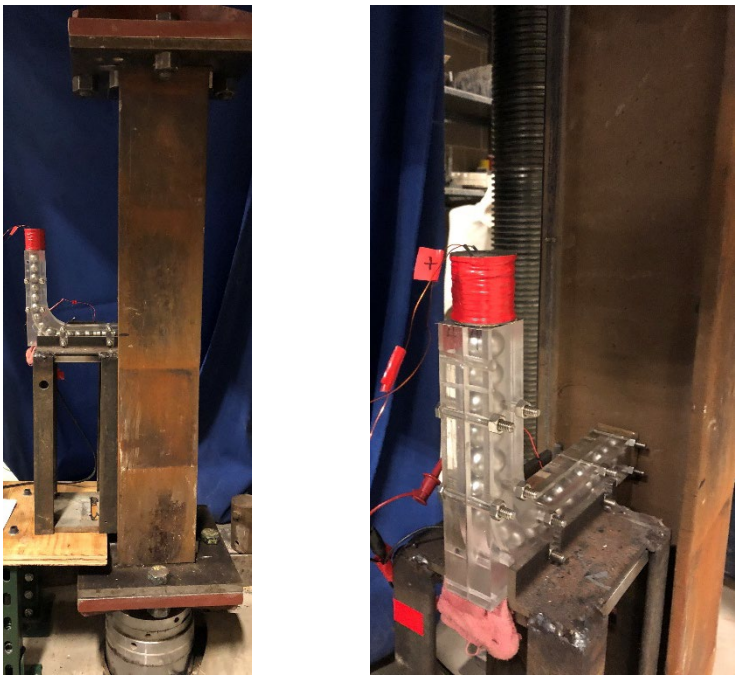

FIGURE 12. Photos of the experimental setup in which an L-shaped transducer probes an AREMA rail 0.9 m long.

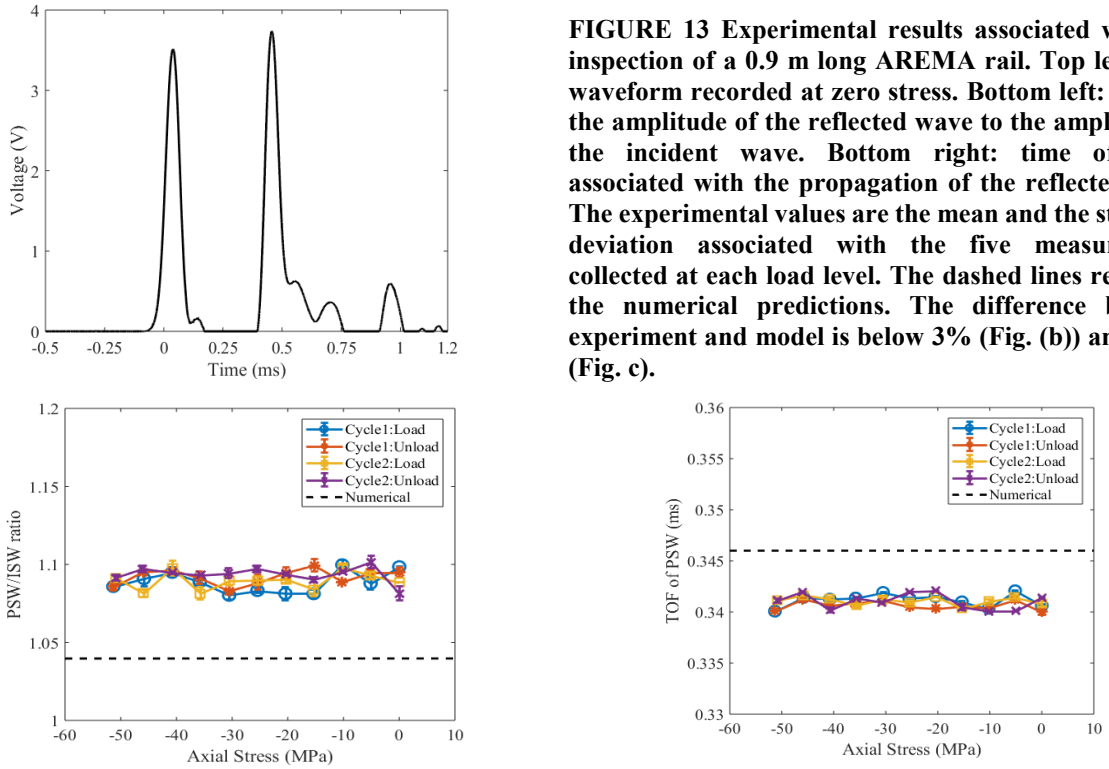

FIGURE 13 Experimental results associated with the inspection of a 0.9 m long AREMA rail. Top left: time waveform recorded at zero stress. Bottom left: ratio of the amplitude of the reflected wave to the amplitude of the incident wave. Bottom right: time of flgiht associated with the propagation of the reflected wave. The experimental values are the mean and the standard deviation associated with the five measurements collected at each load level. The dashed lines represent the numerical predictions. The difference between experiment and model is below 3% (Fig. (b)) and 1.6% (Fig. c).

The results are presented in Fig. 13. Figure 13a shows one of the waveforms recorded at zero stress. As predicted numerically, the secondary wave was absent and the amplitude of the reflected wave was larger than the amplitude of the incident pulse. Not seen in the numerical model, a small hump tailed both the incident and the reflected waves. The origin

of these humps was likely due to the rebound of the striker at the moment of the impact and to some reaction force at the elbow. Figure 13b displays the amplitude ratio as a function of the axial stress for both loading and unloading cycles. Each dot is the average of the ten measurements and the vertical bars are twice the corresponding standard deviation. The plot proves that the measurements were highly repeatable and that the solitary wave feature was, as predicted numerically, unaffected by the stress. Across the stress interval considered in the experiment, the difference between the numerical and the experimental results was below 5%. Similar considerations can be drawn for the time of flight (Fig. 13c): the measurement were highly repeatable and in excellent agreement with the numerical prediction. The mean experimental value of 0.341 ms was only 1.4% lower than the numerical value of 0.346 ms. The excellent match between the model and the experiment highlights the quality of the model and proves that the new NDE method can be applied in the field to any rail profile provided an accurate account of the length of the "equivalent" beam can be obtained.

Similar to Fig. 13, Fig. 14 shows the results relative to the 2.4 m long rail. For this experiment, the actuator consisted of a commercial electromagnet solenoid lift connected directly to the NI-PXI chassis. Mechanical compression was applied at 100 kN increments up to 600 kN, which corresponded to 30% of the critical load. Two load-unload cycles were completed. At the end of each increment, ten measurements were taken and the waveforms were sampled at 5 MHz. The data presented in Fig. 14 represents the average of the measurements taken at any given load. Although the experimental data did not show a monotonic trend, they were in good agreement with the numerical model. The amplitude ratio was on average below 1.0 and the time of flight was between 0.43 ms and 0.47 ms, i.e. well above what observed for the 0.9 rail (Fig. 13c). These results agree with the numerical predictions shown in Fig. 11: as the equivalent length of the rail increases, the amplitude of the reflected pulse is expected to decrease and the time of flight is expected to increase.

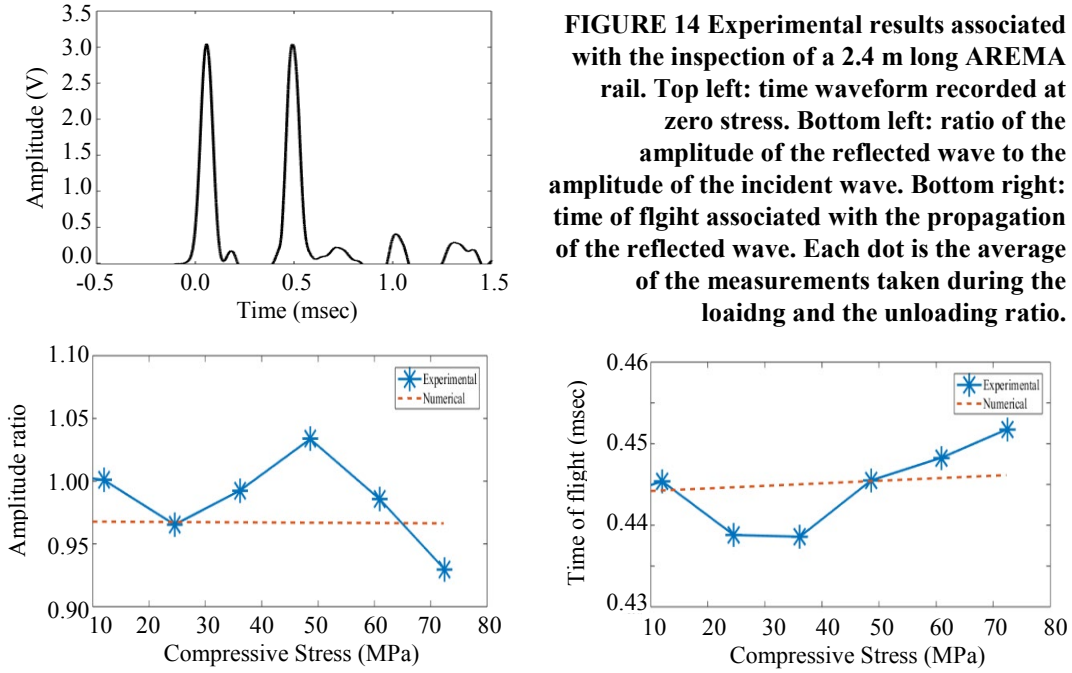

FIGURE 14 Experimental results associated with the inspection of a 2.4 m long AREMA rail. Top left: time waveform recorded at zero stress. Bottom left: ratio of the amplitude of the reflected wave to the amplitude of the incident wave. Bottom right: time of flgiht associated with the propagation of the reflected wave. Each dot is the average of the measurements taken during the loaidng and the unloading ratio.

3.6 DISCUSSION AND CONCLUSIONS ABOUT RAIL TESTING

In this part of the study we investigated numerically and experimentally how the axial stress in rails affects the propagation of highly nonlinear solitary waves along a L-shaped *transducer* in contact with the rail web. The aim was to assess the

reliability of the proposed NDE method at inferring the longitudinal stress in CWRs. The numerical analysis consisted of a finite element model coupled to a discrete particle model. A few features of the solitary waves were observed and charted against the axial stress to identify any variation of the features with respect to the stress. Following common practices, the rail was modeled as "equivalent" to a single beam. Four different beam lenghts were considered, namely 0.9 m, 2.4, 3.6, and 4.8 m. The shortest two rails were examined to be able to compare the numerical results to the experimental results obtained by testing two rail segments under compression. The experiments were threfore extremely significant for this study because they allowed to validate the model. As a matter of fact, the experiments validated all the numerical predictions and the discrepancy between experimental and numerical results was in the order of 1.5-4%. Only physical constraints associated with the loading machine prevented from testing longer rails.

The 3.6 m and 4.8 m long rails were consistent with some models found in the scientific literature in which the structural behavior of railroad tracks subjected to compressive thermal stress was considered equivalent to a straight unconstrained beam 3.6 m and 4.8 m long. The analysis was also extremely significant because it demonstrated that the features extracted from the solitary waves are monotonically dependent on the axial stress, i.e. the numerical results proved that the characteristics of the solitary waves are significantly affected by the axial stress.

Overall, the numerical results demonstrated that the proposed non-invasive system is sensitive to the variation of axial stress if the structural response of railroad tracks can be assumed equivalent to straight beams of identical cross-sectional area and moment of inertia. Overall, it can be concluded that the longer is the "equivalent" beam the more sensitive the proposed method is. The numerical results also implied that the nondestructive method can be applied anytime of the year without the need for day long obervations that would eventually require the crossing of the neutral temperature. In addition, the model presented in this article can be generalized and extended to any rail profile.

4. PROJECT OUTCOMES, PRACTICALITY, AND OUTLOOK

This report presented a novel nondestructive evaluation technique for the determination of longitudinal stress in continuous welded rails. The technique is based on the dynamic interaction between solitary waves propagating along a granular monoatomic chain of spheres and the rail to be inspected. The technique was never explored in rail transportation.

This T-86 project built-up upon the fidnigns obtained by the principal investigator under a Federal Railroad Administration (FRA) grant. In that grant the interaction between thin beams and solitary waves was demonstrated, along with the ability to trigger and sense solitary waves in L-shaped chain of particles (see Table 1 for more details). The findings of the FRA grant were instrumental at supporting the research hypothesis behind the scope of work of this T-86 project and none of the research conducted in this IDEA project overlapped with what accomplished in the FRA grant.

The findings and knowledge gains stemmed from this Transit IDEA project can be summarized as follows.

(1) The *transducers* necessary for the excitation, support, and sensing of solitary waves can be assembled easily and with a high degree of repeatibility.

(2) Off-the-shelf hardware and software can be used to control the *transducers* but alternative electronic equipment can be considered.

(3) An *ad-hoc* general finite element method and a discrete particle model were created to predict the effects that longitudinal stress in rails have on the propagation of the solitary waves. The models allow to quantify the sensitivity

of the proposed NDE method in any rail of any geometric profile probed by any L-shaped or straight *transducer* with any number of particles of any size and modulus.

(4) The models were validated experimentally by testing a thick straight beam and two short rails. In all the experiments the agreement between the numerical and experimental results was very good.

(5) The sensitivity of the solitary wave features to the variation of longitudinal stress depends on the structural behavior of the rail. For rails that can be considered structurally equivalent to unconstrained fixed-fixed single beams over 3.5 meters long, it was found that the solitary waves are monotonically dependent on the axial stress and a quantitiave relationship can be extracted to link the features to the stress. The monotonic behavior guarantees that field measurements of the solitary waves can be used to infer univocally the stress in the rail.

(6) The model suggests that the presence of the cross-ties, fasteners, etc. do not affect the methodology *per se*, but rather affects the equivalent length of the rail.

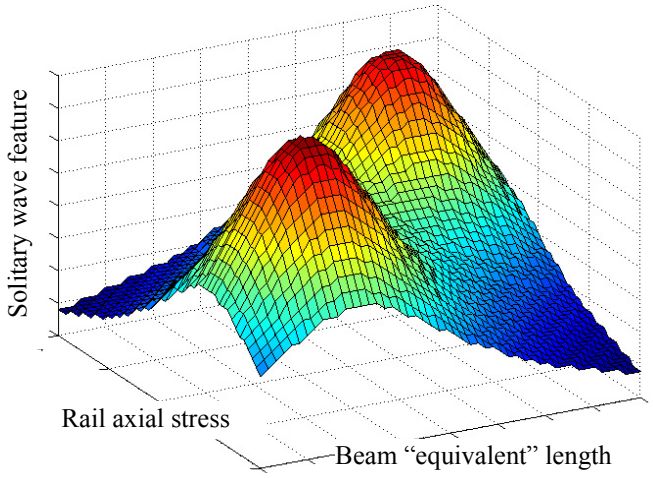

FIGURE 15 – Rendering of a possible 3D plot where a solitary wave feature is charted as a function of the rail axial stress and of the beam "equivalent" length.

Based on the knowledge gained in this T-86 project, the **following recommendations** are warranted for the pathway for field implementation and final demonstration of the technology:

(1) The numerical model should be expanded to create 3-D plots (see a possible example in Fig. 15) in which the solitary wave features are reported as a function of the axial stress and as a function of the "equivalent" beam length.

(2) Laboratory experiments should be carried on longer (4+ m) rails to validate further the models.

(3) Field tests should be taken at real railroad tracks to quantify any discrepancy between the models developed in this project with the "equivalent" beam theories found in the literature. These tests should be taken for several hours to observe the rail under different temperatures, i.e. under different stresses.

(4) Models for curved rails should be developed.

Owing to the knowledge gained in this study, the procedure to adopt ***ANTEUSW*** in the field would be as follows.

STEP 1. The information about the rail profile (size and moment of inertia) and steel (Young modulus E and coefficient of thermal expansion α) is collected and fed into the finite element model.

STEP 2. The output of the model are a set of diagrams in which the solitary waves features (parameter y) are expressed as a function of the variable x (the axial stress $\sigma \equiv x$). Each diagram has a numerical interpolating equations ($y = ax^2+bx+c$),

with the assumption that the given rail is "equivalent" to, let say, a 4.8 meters long single beam. More broadly, a meta-surface and its corresponding equation such as the one shown in Fig. 11 is generated.

STEP 3. In the field, the transducer is placed in contact to the web of the rail to be inspected in order to measure the solitary waves empirically. At the same time, the rail temperature T_R is taken with a thermocouple or with a rail thermometer.

STEP 4. The features y extracted from the time waveform are plugged into the equations $y = ax^2+bx+c$ to solve these equations for the unknown stress σ_R (the variable x).

STEP 5. With the inferred stress σ_R, the neutral temperature T_N is estimated by applying the Equation:

$$T_N = T_R - \frac{\sigma_R}{E\alpha}$$

This estimate would be done having four potential features, namely the time of flight of the primary and the secondary solitary waves; the amplitude ratio of the primary and the secondary solitary waves. This adds redundancy in the NDE system bearing in mind that the variables in the field are the axial stress and the "equivalent length".

Based on the knowledge gained in this project, the proposed NDE method would not require daylong monitoring along which the neutral temperature needs to be crossed. The method does not require the removal of fasteners or to remove crossties. In addition, there is no need for permanent installation of the transducers on the web of the rail. It is noteworthy that the results presented here apply to a *transducer* with the characteristics presented in Fig. 1. However, the model implemented in this study is generalizable: any transducer with any number of spheres of any size and material can be modeled effortlessly.

ANTEUSW, if included in the inspection/maintenance tools of rail operators, may increase the safety of track structures as it may offer a valid tool to estimate the longitudinal stress of CWRs anytime of the year. The knowledge gained in this T-86 project, however, is not sufficient yet to fully guarantee the success of the new method in the field, as it was not tested in real structures. Nonetheless, the accurate models developed in the project, which are based on proven engineering concepts consolidated by the scientific literature, warrant optimism.

5. PLANS FOR IMPLEMENTATION

As this Transit T-86 was a Type 1 project, the Investigators did not included/considered the participation of any transit agency or any rail owner in the actual execution of the project. However, some members of the expert review panel are involved with transit operations and maintenance organizations. The principal investigator believes that the next step for a successful and effective implementation is the execution of a Type 2 project in which:

(1) longer (4+ meters) rails are tested in the lab;

(2) the models are refined to improve the accuracy of the methodology and are extended to curved rails;

(3) one or more *transducers* are deployed in the field in order to monitor real CWRs under different temperatures and to validate the model.

After the completion of the Type 2 project, the long-term vision is to transfer and integrate the new NDE method into a commercial product.

In terms of competitors that may becomes partners, there are a few service providers that developed systems to estimate RNT or applied stress. These providers are potential competitors but none of them currently has the know-how of the proposed method based on the propagation of nonlinear solitary waves.

The customers (market potential) include but are not limited to Transportation Authorities, Rails owners, and governments around the globe. The success of this IDEA project will ease the transition from the laboratory to the field. We have identified some possible commercial partners but no agreements or contracts were sought yet. It is believed that the superior and novel nature of the proposed technology as well as the additional benefits that it brings to customers enables our venture to differentiate the product with respect to potential competitors.

The roadmap of the proposed technology is shown in Fig. 16. A few years ago, the PI proved the proof-of-concept of highly nonlinear solitary waves coupled to thin beams (a few mm wide and thick and a couple of meters long) and investigated the fundamental concepts associated with the propagation of such waves in straight and curved chain of particles. The findings (Ni et al. 2013; Cai et al. 2013a, 2013b; Bagheri et al. 2015a, 2015b; Bagheri et al. 2016a, 2016b) represented the solid evidence that the method may work for thick beams and rails, and were instrumental at supporting the research hypotheses of this Type 1 T-86 project. The results of this project confirmed all the research hypothesis.

ANTEUSW aims to be used with minimum traffic disruption, with a few measurements that do not require day-long observations under favorable weather, and without permanent wayside installations. A major factor in achieving industry acceptance is to demonstrate the new technology in real railroads. As such the next steps of this research include the study of curved rails and the testing of ***ANTEUSW*** in the field in collaboration with railroads owners in order to validate the technology under service traffic.

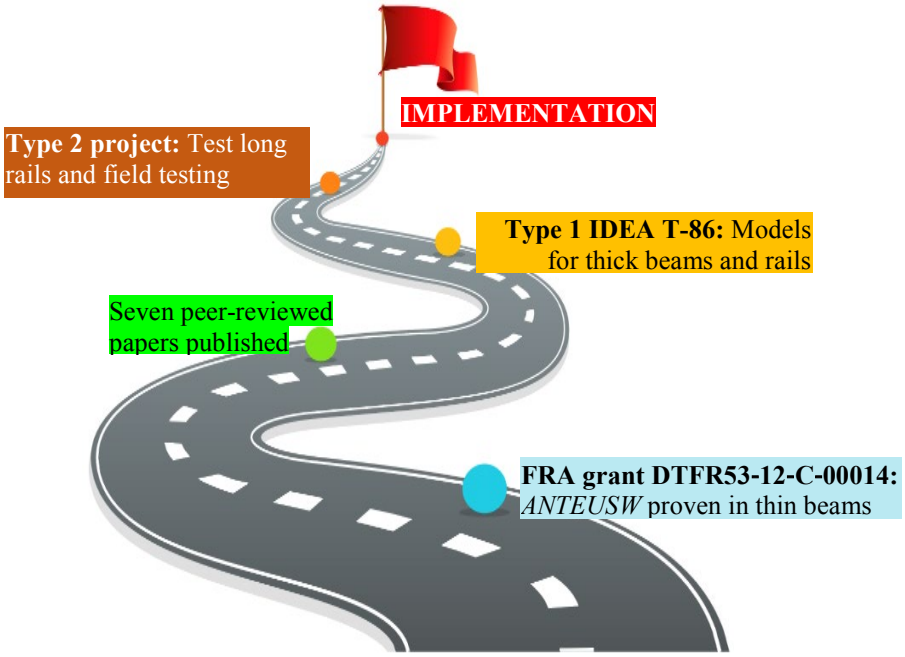

FIGURE 16 Roadmap showing the past, present, and future of ***ANTEUSW***.

6. INVESTIGATORS PROFILE

The Principal Investigator of this T-86 project is Piervincenzo Rizzo, Full Professor in the Department of Civil and Environmental Engineering at the University of Pittsburgh. This project is about NDE, rail inspection, and solitary wave propagation. Dr. Rizzo has 18 years of experience in NDE and structural health monitoring (SHM), about 14 years of experience in research and development of railroad NDE, and about 11 years of experience about the application of highly nonlinear solitary waves for the NDE structural and biological materials. To date, he authored 99 referred papers, 8 book

chapters, and 170+ conference proceedings and abstract, and technical reports. Dr. Rizzo is the first person worldwide who has received both the Achenbach Medal (in 2012) and the SHM Person of the Year Award (in 2015). The Medal recognizes one young individual who has made an outstanding contribution to the advancement of the field of SHM. The Award recognizes accomplishments within the past year or the past few years. Both honors are selected by the editors and associate editors of SHM: An International Journal, the top journal on the subject. The PI received also the 2016 University of Pittsburgh Chancellor's Distinguished Research Junior Scholar Award. The award includes faculty across the whole University, within 12 years from their Ph.D., who have achieved some international standing.

Dr. Rizzo earned a Laurea (5-years degree equivalent to a M.S.) in Aeronautical Engineering from the University of Palermo, Italy. He earned a M.S. and a Ph.D. in Structural Engineering in 2002 and 2004, respectively, from the University of California, San Diego. His doctoral dissertation was on the acoustoelastic effect applied to the determination of applied stress in stay-cables. Thus, he has a wide knowledge on the subject of acoustoelasticity to address the need to determine residual and applied stress. In Fall 2006, he was appointed assistant professor at the University of Pittsburgh's Department of Civil and Environmental Engineering where he founded the Laboratory for NDE and SHM studies. In spring 2012 he was promoted to Associate Professor with tenure, and six years later he was promoted to the rank of Full Professor.

Dr. Rizzo founded and directs the Lab for NDE and SHM Studies. His research has been funded by the National Science Foundation, the Pennsylvania Department of Transportation, the Federal Railroad Administration, the National Academies of Science, and the American Society for Nondestructive Testing, plus a few Pitts' internal grants. Dr. Rizzo was the recipient of the 2002 Fellowship Award, the 2007 Faculty Grant Award, the 2009 Fellowship Research Award, and two ASNT Outstanding Paper Awards (in 2013 and 2017) all from the American Society for Nondestructive Testing. He is one of the very few people that has received two ASNT Outstanding Paper Awards since its inception of this award in the sixties. Finally, Dr. Rizzo was awarded by the Department of Structural Engineering at the University of California, San Diego, with the 2019 Oustanding Distiguished Alumni award.

Dr. Amir Nasrollahi, currently post-doc under the supervision of Dr. Rizzo, worked on the project as graduate student. Dr. Nasrollahi earned a B.S. in Civil Engineering from Azad University (Iran), and a M.S. in Earthquake Engineering from the Road, Housing, and Urban Development Research Center, BHRC Institute, still in Iran. To date, he has published 22 peer-reviewed papers and has presented his research at several international conferences.

REFERENCES

Bagheri, A., Rizzo, P., and Al-Nazer, L. (**2015a**). "Determination of the neutral temperature of slender beams by using nonlinear solitary waves," *ASCE Journal of Engineering Mechanics*, 141(6), 04014163 (8 pages).

Bagheri, A., La Malfa Ribolla, E., Rizzo, P., Al-Nazer, L., and Giambanco, G. (**2015b**). "On the use of L-shaped granular chains for the assessment of thermal stress in slender structures," *Experimental Mechanic*, 55(3), 543-558.

Bagheri, A., Rizzo, P., and Al-Nazer, L. (**2016a**). "A Numerical Study on the Optimization of a Granular Medium to Infer the Axial Stress in Slender Structures," *Mechanics of Advanced Materials and Structures*, 23(10), 1131-1143, DOI: 10.1080/15376494.2015.1039679.

Bagheri, A., La Malfa Ribolla, E., Rizzo, P., and Al-Nazer, L. (**2016b**) "On the coupling dynamics of thermally stressed beams and granular chains," Archives of Applied Mechanics, 86(3), 541-556.

Cai, L., Yang, J., Rizzo, P., Ni, X., and Daraio, C. (**2013a**). "Propagation of Highly Nonlinear Solitary Waves in a Curved Granular Chain," *Granular Matters*, 15(3), 357-366.

Cai, L., Rizzo, P., and Al-Nazer, L. (**2013b**). "On the Coupling Mechanism between Nonlinear Solitary Waves and Slender Beams," *International Journal of Solid Structures*, 50, 4173-4183.

Lim, N.-H., Han, S.-Y., Han, T.-H., and Kang, Y.-J. (2008). "Parametric study on stability of continuous welded rail track-ballast resistance and track irregularity," *Steel Structures*, 8, 171-181.

Nasrollahi, A., and **Rizzo, P.** (2018) "Axial stress determination using highly nonlinear solitary waves," *The Journal of the Acoustical Society of America,* 144, 2201-2212.

Nasrollahi, A., and **Rizzo, P.** (2019) "Dynamic interaction between highly nonlinear solitary waves and rails: Numerical Analysis and Experimental Validation," under review.

Nesterenko, V. (**1983**). "Propagation of nonlinear compression pulses in granular media," Journal of Applied Mechanics and Technical Physics*,* **24(6)**, 733-743.

Nesterenko, V. (**2001**). Dynamics of heterogeneous materials, Springer-Verlag, New York-Berlin-Heidelberg.

Ni, X., Cai, L., and Rizzo, P. (**2013**). "A Comparative Study on Three Different Transducers for the Measurements of Nonlinear Solitary Waves," *Sensors*, 13, 1231-1246; doi:10.3390/s130101231.

Zienkiewicz, O. C., and Taylor, R. L. (**2013**). The finite element method for solid and structural mechanics (7th Edition), Elsevier, Butterworth-Heinemann Publishing Company, Oxford, UK.